PROPERTIES OF GALACTIC DARK MATTER: CONSTRAINTS FROM ASTRONOMICAL OBSERVATIONS

B. BURCH[1] AND R. COWSIK[1]
Physics Department and McDonnell Center for the Space Sciences, Washington University, St. Louis,
MO 63130, USA; bburch@physics.wustl.edu

ABSTRACT

The distributions of normal matter and of dark matter in the Galaxy are coupled to each other as they both move in the common gravitational potential. In order to fully exploit this interplay and to derive the various properties of dark matter relevant to their direct and indirect detection, we have comprehensively reviewed the astronomical observations of the spatial and velocity distributions of the components of normal matter. We then postulate that the phase-space distribution of dark matter follows a lowered-isothermal form and self-consistently solve Poisson's equation to construct several models for the spatial and velocity distributions of dark matter. In this paper, we compute the total gravitational potential of the normal and dark matter components and investigate their consistency with current observations of the rotation curve of the Galaxy and of the spatial and velocity distributions of blue horizontal-branch and blue straggler stars. Even with this demand of consistency, a large number of models with a range of parameters characterizing the dark matter distribution remain. We find that the best choice of parameters, within the range of allowed values for the surface density of the disk 55 $M_\odot$ pc^{-2}, are the following: the dark matter density at the Galactic center $\rho_{DM,c} \approx$ 100–250 GeV cm^{-3}, the local dark matter density $\rho_{DM}(R_0) \approx$ 0.56–0.72 GeV cm^{-3}, and the rms speed of dark matter particles $\langle v_{DM}^2(R_0)\rangle^{1/2} \approx$ 490–550 km s^{-1}. We also discuss possible astronomical observations that may further limit the range of the allowed models. The predictions of the allowed models for direct and indirect detection will be discussed separately in a companion paper.

Key words: dark matter – Galaxy: fundamental parameters – Galaxy: structure

Online-only material: color figures

1. INTRODUCTION

In the study of dark matter, in its role in the formation of structures in the universe, and in its direct and indirect detection, the mass and luminosity distribution of the Milky Way Galaxy plays a central role. Such considerations perhaps began with the contributions of Oort (1932) to the understanding of the problem in terms of the mass model of the Milky Way and are still relevant. The importance of dark matter, especially weakly interacting relics from the big bang (Cowsik & McClelland 1972, 1973; Lee & Weinberg 1977; Kolb & Turner 1990), in the formation and dynamics of galactic systems became well established in the decades following the early 1970s when detailed and critical reviews were written and modeling of the luminosity distributions and kinematic probes of the Galactic potentials were undertaken (Schmidt 1956; Bahcall & Soneira 1980; Caldwell & Ostriker 1981; Rohlfs & Kreitschmann 1988). Since that time, systematic improvements of the mass models have taken place, notably by Dehnen & Binney (1998), who were concerned with shedding light on the spheroidal nature of the Galactic halo. To this end, they calculated the Galactic gravitational potential for an axisymmetric mass model and investigated its concordance with astronomical constraints obtained from the observations including terminal velocities in the inner Galaxy, the rotation curve, Oort constants, satellites of the Milky Way, the local surface density of the disk (Kuijken & Gilmore 1991), etc. Even though the conceptual basis of the mass models has remained more or less the same, significant sophistication in constraining the parameters of the models, such as Bayesian or Markov Chain Monte Carlo

methods, has led to significant progress (Weber & de Boer 2010; McMillan 2011). With progressively improving capabilities in computation, numerical simulations of galaxy formation provide new mass profiles such as that by Navarro et al. (1997), which have provided further stimulus to addressing issues related to the mass models, including forms that avoid the central cusp, which could have been smoothened by baryonic infall (Nesti & Salucci 2013). The phenomenal sensitivities for the direct detection of the particles of dark matter with instruments placed underground (Ahmed et al. 2011; Aprile et al. 2012; Behnke et al. 2011; Archambault et al. 2012; Felizardo et al. 2012) have brought the focus of these studies to the velocity distribution of the dark matter particles, as this is needed for the proper analysis of the signals detected in these experiments. To this end, several authors have adopted the Eddington formula (Binney & Tremaine 2008), which allows the calculation of the velocity distribution of particles that will self-consistently give rise to a spherically symmetric density distribution that generates the spherically symmetric gravitational potential. By approximating the gravitational potential of the Galaxy to be spherically symmetric, the distribution function that will yield a chosen spherically symmetric mass model for the dark matter halo can be determined (Catena & Ullio 2012; Bhattacharjee et al. 2013). It is clear from this brief review that the development of the mass models has progressed systematically and has reached a high level of sophistication.

With these aforementioned developments, mass models have reached an important watershed. To proceed further, one may take recourse to the well-established paradigm in many branches of physics and astrophysics and try to specify the form of the phase-space distribution (PSD) for all the components of the Galaxy, including the dark matter. If this can be achieved,

---

[1] Campus Box 1105, 1 Brookings Drive, St. Louis, MO 63130, USA.

all the quantities of astrophysical interest may be calculated from these distributions. However, this is a far too challenging task at this stage, and one must approach the problem in steps. In this paper, we have adopted an alternative approach (Cowsik et al. 1996) to the modeling of the Galaxy: we start with a functional form for the PSD of dark matter, which is motivated by physical considerations and has parameters that have a direct bearing on the problem at hand. We then take recourse to astronomical data to obtain a parameterized description of the mass distribution of baryonic (visible) matter in the Galaxy. We then calculate, *self-consistently*, how dark matter with the specified PSD will distribute itself in the gravitational potential generated by the dark matter itself and that generated by the visible matter in the Galaxy. Then, the same set of kinematic and other constraints derived from astronomical observations used in constraining the mass models is used to derive the parameters of the PSD. This approach has not been used extensively, but the earlier studies have indicated some benefits to having a physically motivated distribution function on hand to address the problems related to direct and indirect detection of dark matter. Even this restricted approach already allows us to estimate, for example, the allowed range of the dark matter densities in the central regions of the Galaxy, a parameter difficult to obtain from other methods that rely exclusively on the kinematic indicators like dispersion of the bulge stars and rotation curves in the central regions of the Galaxy, which are dominated by the visible matter distributions in those regions. The PSD is the same throughout the Galaxy and as such can efficiently probe the properties of the system in the entire region accessed by the dynamical trajectories.

As stated above, though the precise PSD of Galactic dark matter is still not well understood, much effort has been invested in understanding the distribution and dynamics of dark matter in the Milky Way for the purposes of understanding the overall dynamics and structure of our Galaxy, as well as for the planning and interpretation of their direct and indirect detection. Most studies assume the framework of the Standard Halo Model of dark matter, which envisages the Milky Way as embedded in an isothermal dark matter halo described by a Maxwell–Boltzmann PSD (often without ensuring self-consistency) with a local dark matter density of 0.3 GeV cm^{-3} and a velocity dispersion of 270 km s^{-1}, and the radial distribution of its density is truncated at the "virial radius" to keep the mass of the halo and the escape velocity finite. However, it is well understood that a Maxwellian distribution is not appropriate for the description of Galactic dark matter (Kuhlen et al. 2010), as it leads to infinite spatial extent and a total mass for the system that indefinitely increases linearly at large distances. Also, recent attempts to estimate the local dark matter density lead to a wide range of values ~0.2–0.6 GeV cm^{-3}: ~0.39 GeV cm^{-3} (Catena & Ullio 2010), 0.2–0.4 GeV cm^{-3} (Weber & de Boer 2010), 0.40 ± 0.04 GeV cm^{-3} (McMillan 2011), 0.43±0.11±0.10 GeV cm^{-3} (Salucci et al. 2010), 0.3 ± 0.1 GeV cm^{-3} (Bovy & Tremaine 2012). In this paper, we carry out a self-consistent calculation of the spatial distribution of dark matter, including the effects of the background gravitational potential generated by the baryonic matter in the Galaxy. Comparison of the predictions of the self-consistent model with various kinematic observables constrains the parameters characterizing the PSD of Galactic dark matter. This allows us to derive the density distribution and other properties pertaining to Galactic dark matter particles in a self-consistent way.

We follow the basic strategy for probing the PSD of dark matter developed by Cowsik et al. (1996). The distributions of dark matter and visible matter are coupled to each other as they are both influenced by the common gravitational potential of the Galaxy, to which each component makes its own contribution. Thus, when we have at hand the density distribution of visible matter, determined by astronomical observations, it is a straightforward matter to calculate the gravitational potential generated by visible matter. Then, for any assumed functional form for the PSD of dark matter, with a given a set of parameters, we can solve the non-linear Poisson equation to determine the potential contributed by dark matter. Thus, having determined the total potential of the Galaxy, we may then use astronomical probes like the rotation curve of the Galaxy and the velocity and spatial distribution of stars to determine the values of the parameters characterizing the PSD function of dark matter that provide good fits to these observations.

The accuracy of determination of the parameters characterizing the PSD of Galactic dark matter depends primarily on the accuracy and extent of astronomical data. Accordingly, the observations of the distribution of the various visible mass components of the Milky Way are reviewed in detail, and correspondingly, a simple axisymmetric model of the density distribution of the Galactic stars and gas is constructed. The particles of dark matter move in the gravitational potential generated by the visible matter and by their own mass distribution, and their spatial distribution is generally assumed to be cut off at the "virial radius," defined as the radius of a sphere that has an average density of Δ times the critical density. The value of Δ suggested by different authors ranges from $\Delta = 200$ (McMillan 2011) to $\Delta = 355$ (Libeskind et al. 2011) or more. However, our analysis indicates that many of the parameters of the PSD function of dark matter are only weakly sensitive to this choice. Assuming a lowered-isothermal PSD for Galactic dark matter, the gravitational potential from dark matter is computed from iterative, self-consistent, solutions of Poisson's equation, following a method adopted by Cowsik et al. (1996). In this way, many dark matter profiles are generated with a wide range of properties depending on the choice of the parameters specifying their PSD. These models are then compared in turn with the current observations of the Galactic rotation curve and to recent observations of the velocity and spatial distribution of blue horizontal-branch (BHB) and blue straggler (BS) stars in the outer Galaxy. Comparing the dark matter models with the rotation curve and with the BHB/BS distributions separately allows for a wide range of dark matter properties. On the other hand, when we demand that the models fit both these simultaneously for the same choice of parameters, the parameter space narrows and becomes almost exclusively dependent on the value chosen for the surface density and scale lengths of the visible disk of the Galaxy. However, even in the combined analysis of the rotation curve and the stellar distributions, a significant range of parameters for the PSD of dark matter is still allowed. Within the current estimates of the mass of the Galactic disk, we find that the best estimates for the local dark matter density are ~0.56–0.72 GeV cm^{-3} with the value of the density at the Galactic center ranging from 100 to 250 GeV cm^{-3}. The escape speed from the center of the Galaxy lies in the range ~940–980 km s^{-1}, and the rms speed of dark matter particles in the solar neighborhood is found to be ~490–550 km s^{-1} for the most favored models.

2. THE VISIBLE MATTER DISTRIBUTION

In order to derive the Galactic dark matter distribution, the distribution of visible matter in the Galaxy must be well

understood, as it is their interplay that allows us to probe the dark matter. We have completed an extensive survey of the current observations of the distributions of stars and gas in the Milky Way and constructed a simple axisymmetric model of the Galaxy that agrees with current data. The known mass distribution of the Galaxy derives contributions from the central black hole, central bulge, disk, and stellar halo populations. In this analysis, the stellar halo is neglected because its contribution to the visible matter density is on the order of 0.1% at R_0, the distance from the Sun to the Galactic center (Helmi 2008), and it is therefore expected to contribute negligibly to the dynamics of the Galaxy. Likewise, the black hole and nuclear bulge, while playing important roles very close to the Galactic center, contribute negligibly to the overall dynamics of the Galaxy in the regions of interest. For the purposes of computing the gravitational potential in this paper, the visible Galaxy consists of a central bulge and a thin and a thick exponential disk. There are several ways to model these components, and here, models that most closely fit the observations of the stars and gas are adopted.

2.1. The Disk

The mass densities of both the thin (tn) and the thick (tk) disk components are typically modeled as double-exponential functions with early evidence for their validity given by Freeman (1970). Following the notation used in many recent analyses (Cabrera-Lavers et al. 2005; McMillan 2011), the densities for the separate components may be written as

$$\rho_{tn}(r,z) = \frac{\Sigma_{tn,c}}{2z_{tn}} e^{-|z|/z_{tn}} e^{-r/r_{tn}}, \qquad (1)$$

$$\rho_{tk}(r,z) = \frac{\Sigma_{tk,c}}{2z_{tk}} e^{-|z|/z_{tk}} e^{-r/r_{tk}}, \qquad (2)$$

$$\rho_d = \rho_{tn} + \rho_{tk}, \qquad (3)$$

$$\Sigma_d = \Sigma_{tn} + \Sigma_{tk}, \qquad (4)$$

in cylindrical coordinates, where ρ_d is the total density of the Galactic disk, $\Sigma_{tk/tn,c}$ are the surface densities near the Galactic center (including both stars and gas), $z_{tk/tn}$ are the scale heights, and $r_{tk/tn}$ are the radial scale lengths for the thick and thin components, respectively. The masses of the two components are given by

$$M_{tk/tn} = 2\pi \Sigma_{tk/tn,c} r_{tk/tn}^2. \qquad (5)$$

For the total local surface density at R_0 from visible matter, we consider the values $\Sigma_{d,\odot} = 40$, 55, and 70 $M_\odot$ pc^{-2}, which is within the range found in the literature (Kuijken & Gilmore 1989, 1991; Flynn & Fuchs 1994; Gould et al. 1996; Korchagin et al. 2003; Siebert et al. 2003; Holmberg & Flynn 2004; Flynn et al. 2006; Weber & de Boer 2010). For convenience, the ratio of the thick disk surface density at R_0 to the total surface density at R_0 is taken to be

$$\frac{\Sigma_{tk,\odot}}{\Sigma_{tk,\odot} + \Sigma_{tn,\odot}} = 0.1, \qquad (6)$$

a value that is also within the range of the findings of many studies (Ohja 2001; Reid & Majewski 1993; Buser et al. 1999;

Spagna et al. 1996; Ng et al. 1997; Larsen & Humphreys 2003; Robin et al. 1996; Siegel et al. 2002; Carollo et al. 2010). The choice of the ratio in Equation (6), within observational constraints, does not have a significant effect on the rotation curve or other dynamical indicators calculated in this paper.

From the compilation of observations, a complete range in the radial scale length of the thin disk $r_{tn} = 2.0$, 2.5, 3.0, and 3.5 kpc was considered, and r_{tk} was taken to be 3.5 kpc, though there is recent evidence that the radial scale length of the thick disk could be as short as ~ 2 kpc (Bensby et al. 2011; Cheng et al. 2012; Bovy et al. 2012b). The scale heights are chosen to be $z_{tn} = 350$ pc and $z_{tk} = 900$ pc, close to the values determined by Jurić et al. (2008), and are seen to not have a strong effect on the calculated rotation curve, agreeing with the analysis of McMillan (2011). The above parameters yield a combined disk mass in the range $(3.57$–$6.24) \times 10^{10} M_\odot$. Note, this simple disk model does not include some of the finer structures of the disk such as the spiral arms or the warp included in other analyses (Sofue et al. 2009) since an axisymmetric model is adequate to describe the overall dynamics and accords computational simplicity.

The disk potential has the form (Kuijken & Gilmore 1989; Mo et al. 2010)

$$\Phi_d(r,z) = -2\pi G \left(\Sigma_{tn,c} r_{tn}^2 \int_0^\infty dk \frac{J_0(kr)}{[1+(kr_{tn})^2]^{3/2}} \right.$$
$$\times \frac{e^{-k|z|} - (kz_{tn})e^{-|z|/z_{tn}}}{1-(kz_{tn})^2} + \Sigma_{tk,c} r_{tk}^2 \int_0^\infty dk$$
$$\left. \times \frac{J_0(kr)}{[1+(kr_{tk})^2]^{3/2}} \frac{e^{-k|z|} - (kz_{tk})e^{-|z|/z_{tk}}}{1-(kz_{tk})^2} \right). \qquad (7)$$

Note that the potential includes integration over Bessel functions, $J_0(kr)$, which slows down numerical calculations of the rotation curve for the different models. We find that using an adaptive quasi-Monte-Carlo method in *Mathematica* provides the quickest computation time without sacrificing accuracy.

2.2. The Bulge

The bulge, in cylindrical coordinates, is described by a Plummer density profile of the form

$$\rho_b = \frac{3M_b}{4\pi b^3} \left(1 + \frac{r^2+z^2}{b^2} \right)^{-5/2}, \qquad (8)$$

where M_b is the total mass of the bulge and b is the scale radius. To determine M_b and b, we assume that the dark matter contribution to the dynamics from ~ 0.1–1 kpc is small (an assumption that implies that visible matter dominates the dynamics in the very central regions of the Galaxy and is justified post facto) and subtract the disk contribution from the inner 1 kpc. Noting that the contributions of various components to $v_c^2(r)$ are additive, we subtract the theoretically expected contribution to $v_c^2(r)$ from the square of the observed values for $r \lesssim 1$ kpc to obtain the exclusive contribution of the bulge. The resulting points are fit with the rotation curve derived from the Plummer density. The bulge parameters are found to be $M_b = 1.02 \times 10^{10} M_\odot$ and $b = 0.258$ kpc. The potential of the Plummer model has the simple analytical form

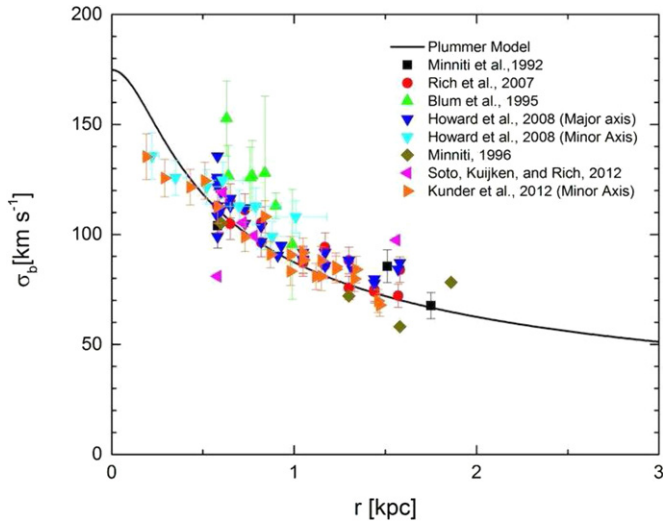$$\Phi_b = -\frac{GM_b}{(r^2+z^2+b^2)^{1/2}} \qquad (9)$$

Figure 1. Velocity dispersion expected from the bulge (Equation (10)) is plotted along with K and M giant observations (Minniti et al. 1992; Rich et al. 2007; Blum et al. 1995). The agreement between the observations and the prediction from the Plummer profile implies that the mass distribution of the bulge can be adequately fit by a Plummer profile in the region of interest.

(A color version of this figure is available in the online journal.)

and a velocity dispersion (Dejonghe 1987) given by

$$\sigma_b^2 = \frac{GM_b}{6(r^2 + z^2 + b^2)^{1/2}}. \tag{10}$$

We show the velocity dispersion in Figure 1, along with measurements of K and M bulge giants (Minniti et al. 1992; Rich et al. 2007; Blum et al. 1995). Note that the dispersion expected from the Plummer model agrees well with the observations, implying that this region is adequately described by a bulge-dominated density profile. Including the mass contribution from the disk in the bulge region does not noticeably change the predictions for the velocity dispersion.

3. KINEMATIC OBSERVATIONS: THE ROTATION CURVE AND STELLAR VELOCITY DISTRIBUTIONS

Recent observations of stars, interstellar gas, and masers have been able to extend our understanding of the dynamics of the Galaxy beyond the solar circle, as well as improving observations near the solar location. The density and dynamics of these objects probe the Galactic gravitational potential. The gravitational potential in the Galactic plane as a function of the distance from the Galactic center can be determined from the rotational speed of the Galaxy in the usual way:

$$\frac{v_c^2}{r} = \left| \frac{\partial \Phi_{\text{tot}}}{\partial r} \right|, \tag{11}$$

where Φ_{tot} is the total gravitational potential of the Galaxy, obtaining contributions from both its visible and dark matter components. The best observations of the Milky Way's rotation curve now span the range of galactocentric distances $\sim$1–20 kpc. The Galactic potential can be probed up to $\sim$90 kpc by considering the velocity distribution of BHB and BS stars. Recent compilations of carefully selected BHB stars by Xue et al. (2008) and BHB and BS stars by Brown et al. (2010) are used below to constrain the Galactic dark matter distribution.
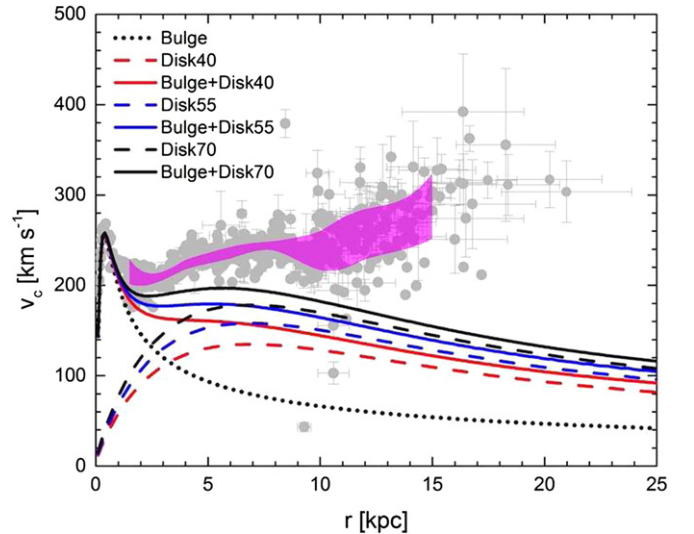

Figure 2. Observations of the rotation curve (Burton & Gordon 1978; Blitz et al. 1982; Schneider & Terzian 1983; Clemens 1985; Fich et al. 1989; Burton & Liszt 1993; Turbide & Moffat 1993; Honma & Sofue 1997; Pont et al. 1997; Honma et al. 2007; McClure-Griffiths & Dickey 2007; Oh et al. 2010; Stepanishchev & Bobylev 2011) are plotted after rescaling all the data using $R_0 = 8.3$ kpc and $\Theta_0 = 240$ km s^{-1} and adjusting for the current measurements of the peculiar motion of the Sun. The magenta band indicates there region where 2/3 of the points lie within 1 kpc radial bins. The rotation curve predicted by the visible matter components alone for the three local disk surface densities with $r_{\text{tn}} = 3.0$ kpc is shown along with the shaded observations.

(A color version of this figure is available in the online journal.)

3.1. The Rotation Curve

The best estimates of the gravitational potential in the Galactic plane within $\sim$10 kpc of the Galactic center come from measurements of the Galactic rotation speed. We have compiled a large sample of the available observations (Burton & Gordon 1978; Blitz et al. 1982; Schneider & Terzian 1983; Clemens 1985; Fich et al. 1989; Burton & Liszt 1993; Turbide & Moffat 1993; Honma & Sofue 1997; Pont et al. 1997; Honma et al. 2007; McClure-Griffiths & Dickey 2007; Oh et al. 2010; Stepanishchev & Bobylev 2011), excluding only those with exceptionally high dispersion in the data (Demers & Battinelli 2007). The rotation curve inside the solar circle is well determined by observations of H I regions and CO emission associated with H II regions. Outside the solar circle, distances to objects are much more difficult to measure accurately, so the errors in the rotation curve are correspondingly larger. We present a compilation of the data used in our analysis in Figure 2, with error bars when available, along with a medial shaded band, which includes 2/3 of the data points in 1 kpc radial bins and the rotation curve from the visible components of our Galactic mass models with $r_{\text{tn}} = 3$ kpc.

The Milky Way's rotation curve is derived from line-of-sight observations of interstellar hydrogen and other material like CO, masers, planetary nebula, and other astrophysical objects. The determination of the rotation curve of the Galaxy depends on the assumed value of R_0, the distance from the Galactic center to the Sun, and Θ_0, the rotation speed of the Sun about the Galactic center. Recently, maser observations and measurements of stellar orbits near SgrA* have been able to constrain $R_0 = 7.2$–9 kpc (Ghez et al. 2008; Gillessen et al. 2009; Reid 2009; Reid et al. 2008; Brunthaler et al. 2011). A summary of some estimates of R_0 can be found in Avedisova (2005). We choose $R_0 = 8.3$ kpc based on these and other

stellar observations from the past decade. The ratio Θ_0/R_0 is well constrained from masers and stellar orbits (Reid 2009; Brunthaler et al. 2011; Reid & Brunthaler 2004) and is in the range of $\Theta_0/R_0 = 28.5$–30.3 km s^{-1} kpc^{-1}. We take $\Theta_0/R_0 \approx 28.9$ km s^{-1} kpc^{-1} such that $\Theta_0 = 240$ km s^{-1}. This value of Θ_0 differs significantly from the IAU standard values (see McMillan & Binney 2010 and the references therein) of $R_0 = 8.5$ kpc and $\Theta_0 = 220$ km s^{-1}, which gives $\Theta_0/R_0 \approx 25.9$ km s^{-1} kpc^{-1} and does not agree with the recent observations of masers and stellar orbits. There are, however, some recent studies that call into question this high value of Θ_0 (Koposov et al. 2010; Bovy et al. 2012a), preferring values closer to 220 km s^{-1}. The result of reanalyzing the observations using the larger value of Θ_0 is that the rotation curve gently rises from ~2–15 kpc instead of remaining flat, and correspondingly, the density of dark matter needed to reconcile the theoretically computed rotation curve with the data increases. We have also corrected all the rotation curve data taking account of the new measurements of the peculiar motion of the Sun $(U_\odot, V_\odot, W_\odot)$, where $V_\odot$ has been updated from ~5 km s^{-1} to ~11–15 km s^{-1} (McMillan & Binney 2010; Schönrich et al. 2010). We take $(U_\odot, V_\odot, W_\odot) = (11, 12, 7.5)$ km s^{-1}.

3.2. Blue Horizontal-branch Stars

Xue et al. (2008) have compiled an extensive list of the line-of-sight velocities of 2401 BHB stars from the Sloan Digital Sky Survey DR6, taking care to ensure that their sample is pure and contains accurate data on both the distance and line-of-sight velocity of each star. They use these data to constrain cosmological simulations and estimate the virial mass of the Galaxy, as well as derive the rotation curve up to ~60 kpc. We combine their compilation of 2401 BHB stars within 60 kpc of the Galactic center with their separate compilation of stars at galactocentric distances of ~60–90 kpc. This combined compilation extends from 5 to 90 kpc with line-of-sight velocities spanning ± 350 km s^{-1}. After rescaling the galactocentric distances and line-of-sight velocities for each star to correspond to the values of R_0 and Θ_0 chosen above, the observations are divided into 11 radial bins where the positive and negative radial velocities are averaged and divided into 50 km s^{-1} bins. Error bars are shown as $\pm\sqrt{N}$, where N is the average number of stars in each velocity bin.

Brown et al. (2010) have compiled a sample of 910 BHB and BS stars from the Hypervelocity Star Survey, which contains twice as many stars at $r \geqslant 50$ kpc compared to the compilations by Xue et al., and they derive the velocity dispersion profile of the Milky Way out to ~95 kpc. While the Brown et al. sample claims to be complete in color, magnitude depth, and spatial coverage, there is some ambiguity in distinguishing BHB from BS stars. To achieve the ratio of BHB to BS stars as stated in Brown et al., stars with $f_{BHB} \geqslant 0.6$ were taken to be BHB stars, where f is the likelihood of a candidate star being a BHB star as reported in Table 1 of Brown et al., and any star with $f_{BHB} < 0.6$ was considered to be a BS star. This reproduces the 74%-to-26% BHB-to-BS ratio in Brown et al. As with the stars in the compilation by Xue et al., this sample too was rescaled for our adopted values of R_0 and Θ_0. We find that we are unable to reproduce the R_{BHB} and R_{BS} distances in Table 1 of Brown et al. (2010) for their choice of R_0, Θ_0, and $(U_\odot, V_\odot, W_\odot)$. We calculate the heliocentric distance for the BHB and BS stars using Equation (2) in Brown et al. and convert it to a galactocentric distance in the usual way (see Equation (4) in Xue et al. 2008). The stellar observations are then divided into

eight radial bins. The line-of-sight velocities are averaged, and the error bars are determined in the same manner as for the Xue et al. distribution.

4. THE GALACTIC DARK MATTER DISTRIBUTION

The density distribution of dark matter is controlled by both the velocity distribution of the dark matter particles and the total gravitational potential Φ_{tot} in which they reside. The total potential receives contributions from the density distributions of both the visible and the dark matter components of the Galaxy:

$$\Phi_{tot} = \Phi_b + \Phi_d + \Phi_{DM}, \tag{12}$$

where Φ_b, Φ_d, and Φ_{DM} are the potentials contributed by the bulge, the disk, and the dark matter, respectively. In order to develop a self-consistent model for the dark matter in our Galaxy, we require a dynamical model whose PSD function represents a collisionless system that can be parameterized by the velocity dispersion of the dark matter, the density either at the Galactic center or at R_0, and the size of the dark matter halo. A lowered isothermal (King) distribution is well suited for this and is described in Binney & Tremaine (2008). Unlike the isothermal sphere, the King distribution has a finite total mass, a non-singular central density, and meets all the requirements of the model. Reasons for choosing the King distribution are also discussed in earlier papers (Cowsik et al. 2007; Chaudhury et al. 2010).

The distribution function for the King model is given by

$$f_K(\varepsilon) = \begin{cases} \dfrac{\rho_1}{\left(2\pi\sigma_{DM}^2\right)^{3/2}}(e^{\varepsilon/\sigma_{DM}^2} - 1) & \text{for } \varepsilon > 0 \\ 0 & \text{for } \varepsilon \leqslant 0, \end{cases} \tag{13}$$

where

$$\varepsilon \equiv \Phi_0 - \left(\frac{1}{2}v^2 + \Phi_{tot}\right). \tag{14}$$

The parameter Φ_0 is the potential at $r = r_t$, the "virial" (King) radius of the dark halo, and ρ_1 and σ are parameters that are related but not equal to the central dark matter density $\rho_{DM,c}$ and the dark matter velocity dispersion, respectively.

The dark matter density distribution is readily calculated by integrating the distribution function,

$$\rho_{DM} = \int f_K d^3v, \tag{15}$$

and vanishes at $r = r_t$ where $\varepsilon = 0$. Defining the scaled potential $\Psi(r, z)$ as

$$\Psi(r, z) \equiv \Phi_0 - \Phi_{tot}(r, z), \tag{16}$$

the density distribution of dark matter may be written as

$$\rho_{DM}(\Psi(r, z)) = \frac{\rho_1}{\left(2\pi\sigma_{DM}^2\right)^{3/2}} \int_0^{\sqrt{2\Psi(r,z)}} dv v^2$$
$$\times \left[\exp\left(\frac{\Psi(r,z) - \frac{1}{2}v^2}{\sigma_{DM}^2}\right) - 1 \right]$$
$$= \rho_1 \left[e^{\Psi(r,z)/\sigma_{DM}^2} \text{erf}\left(\frac{\sqrt{\Psi(r,z)}}{\sigma_{DM}}\right) \right.$$
$$\left. - \sqrt{\frac{4\Psi(r,z)}{\pi\sigma_{DM}}} \left(1 + \frac{2\Psi(r,z)}{3\sigma_{DM}^2}\right) \right]. \tag{17}$$

Table 1
Dark Matter Model Parameters and Derived Quantities for the $r_{\rm tn} = 2.5$ and $\Sigma_{d,\odot} = 40\ M_\odot\ {\rm pc}^{-2}$ Disk

$\rho_{{\rm DM},c}$ (GeV cm^{-3})	25	50	75	100	250	500
$\sigma_{\rm DM}$ (km s^{-1})	⋯	240	225	220	205	⋯
	⋯	⋯	230	225	⋯	⋯
$\Psi_0/\sigma_{\rm DM}^2$	⋯	8	9	9	10	⋯
	⋯	⋯	9	9	⋯	⋯
$v_{\rm esc}(0)$ (km s^{-1})	⋯	960	955	933	917	⋯
	⋯	⋯	976	955	⋯	⋯
$v_c(R_0)$ (km s^{-1})	⋯	246	241	242	243	⋯
	⋯	⋯	250	252	⋯	⋯
$\langle v_{\rm DM}^2(R_0)\rangle^{1/2}$ (km s^{-1})	⋯	522	515	487	454	⋯
	⋯	⋯	534	506	⋯	⋯
$\rho_{\rm DM}(R_0)$ (GeV cm^{-3})	⋯	0.723	0.644	0.632	0.573	⋯
	⋯	⋯	0.737	0.726	⋯	⋯
$v_{\rm esc}(R_0)$ (km s^{-1})	⋯	673	665	629	586	⋯
	⋯	⋯	689	653	⋯	⋯
$M_{\rm galaxy}$ ($10^{12}\ M_\odot$)	⋯	1.54	1.64	1.34	1.10	⋯
	⋯	⋯	1.71	1.40	⋯	⋯
L	⋯	0.274	0.652	0.093	0	⋯
	⋯	⋯	0.746	0.173	⋯	⋯

Table 2
Dark Matter Model Parameters and Derived Quantities for the $r_{\rm tn} = 3.0$ and $\Sigma_{d,\odot} = 40\ M_\odot\ {\rm pc}^{-2}$ Disk

$\rho_{{\rm DM},c}$ (GeV cm^{-3})	25	50	75	100	250	500
$\sigma_{\rm DM}$ (km s^{-1})	⋯	⋯	⋯	⋯	205	195
$\Psi_0/\sigma_{\rm DM}^2$	⋯	⋯	⋯	⋯	11	12
$v_{\rm esc}(0)$ (km s^{-1})	⋯	⋯	⋯	⋯	962	955
$v_c(R_0)$ (km s^{-1})	⋯	⋯	⋯	⋯	250	244
$\langle v_{\rm DM}^2(R_0)\rangle^{1/2}$ (km s^{-1})	⋯	⋯	⋯	⋯	515	498
$\rho_{\rm DM}(R_0)$ (GeV cm^{-3})	⋯	⋯	⋯	⋯	0.760	0.662
$v_{\rm esc}(R_0)$ (km s^{-1})	⋯	⋯	⋯	⋯	665	643
$M_{\rm galaxy}$ ($10^{12}\ M_\odot$)	⋯	⋯	⋯	⋯	1.61	1.62
L	⋯	⋯	⋯	⋯	0.777	0.791

Note. See the caption of Table 1 for details.

Notes. In the above and following tables, the dark matter at the center of the Galaxy, $\rho_{{\rm DM},c}$, and the parameters $\sigma_{\rm DM}$ and $\Psi_0/\sigma_{\rm DM}^2$ are the free parameters for the lowered-isothermal model of the phase-space distribution of Galactic dark matter, as explained in Section 4. We also show the following derived quantities: the escape speed from the Galactic center, $v_{\rm esc}(0)$, the rotation speed at the solar location, $v_c(R_0)$, the rms velocity of dark matter particles at the solar location, $\langle v_{\rm DM}^2(R_0)\rangle^{1/2}$, the local dark matter density, $\rho_{\rm DM}(R_0)$, the escape speed from the solar location, $v_{\rm esc}(R_0)$, and the total mass of the Galaxy including both visible and dark matter, $M_{\rm galaxy}$. Also shown is the Poisson likelihood L (Equation (25)) computed by comparing predictions from the dark matter models to the radial and velocity distributions of BHB and BS stars, as explained in Section 5.2. For a given value of $\rho_{{\rm DM},c}$, entries with two values of $\sigma_{\rm DM}$ indicate instances where both values of $\sigma_{\rm DM}$ had corresponding rotation curves that were consistent with 2/3 of the available observations. We show the derived quantities for both values of $\sigma_{\rm DM}$.

Note that $\sqrt{2\Psi(r,z)}$ is just the escape speed from the Galaxy of particles at (r, z).

Keeping in mind that $\rho_{\rm DM}$, which is the source for $\Phi_{\rm DM}$, depends on $\Phi_{\rm DM}$ itself, the dark matter potential must be calculated iteratively by numerically solving the Poisson equation,

$$\nabla^2 \Phi_{\rm DM}(r, z) = 4\pi G \rho_{\rm DM}(r, z), \qquad (18)$$

with $\rho_{\rm DM}(r, z)$ given by Equation (17). The procedure that we adopt here is a Legendre polynomial expansion as described in Cowsik et al. (1996), which is based on the earlier work by Wilson (1975) and Prendergast & Tomer (1970). In this way, we produce the density and gravitational potential for visible matter and dark matter separately, as well as for the sum of the two components.

For the above calculations, we formulate the King distribution in terms of $\sigma_{\rm DM}$, $\rho_{{\rm DM},c}$, and $\Psi_0/\sigma_{\rm DM}^2$, where $\Psi(r = 0, z = 0) = \Psi_0$. The precise choices for σ, $\rho_{{\rm DM},c}$, and $\Psi_0/\sigma_{\rm DM}^2$ are made after solving Equation (18) for a range of values, calculating the corresponding rotation curve (Equation (19)), and comparing the results to the observations of the rotation curve and the velocity distribution of BHB and BS stars.

5. COMPARISON WITH ASTRONOMICAL OBSERVATIONS

In order to compare model predictions with the observed rotation curve and the observations of spatial and velocity distributions of BHB and BS stars, a large sample of possible dark matter models was generated, with values chosen by hand, encompassing $\rho_{{\rm DM},c} = 1$–1000 GeV cm^{-3} (we consider 1, 5, 10, 25, 50, 75, 100, 250, 500, and 1000 GeV cm^{-3}), $\sigma_{\rm DM} \approx 100$–1000 km s^{-1} (in 5 km s^{-1} intervals), and $\Psi_0/\sigma_{\rm DM}^2 \approx$ 1–25 (in unit intervals) for each of the 12 disks models. For each model, $\Psi(r, z)$, $\rho_{\rm DM}(R_0)$, $\langle v_{\rm DM}^2(R_0)\rangle^{1/2}$, $v_c(R_0)$, the escape velocity $v_{\rm esc}$, and the total mass of the Galaxy $M_{\rm Galaxy}$ are calculated. Bounds were first put on the parameters of the models by placing the constraint 220 km s$^{-1} \leqslant v_c(R_o) \leqslant 260$ km s^{-1}. Then, models that agreed with the rotation curve were found within these bounds.

5.1. Comparison with the Rotation Curve

The very discovery of dark matter in the Galaxy and the subsequent determinations of its characteristics rest almost exclusively on the measurements of the rotation curve. In this section, we compare the sequence of models that we have calculated with our compilation of observations shown in Figure 2 to limit the range of parameters characterizing the PSD function of dark matter. The theoretical estimates of the rotational velocities are calculated using the expression

$$v_c(r) = \left(r \frac{\partial \Phi_{\rm tot}(r, 0)}{\partial r} \right)^{1/2}$$
$$= \left(r \frac{\partial}{\partial r} [\Phi_b(r, 0) + \Phi_d(r, 0) + \Phi_{\rm DM}(r, 0)] \right)^{1/2} \quad (19)$$

for the 12 sets of models characterized by the three choices of $\Sigma_{d,\odot} = 40\ M_\odot\ {\rm pc}^{-2}$, $55\ M_\odot\ {\rm pc}^{-2}$, and $70\ M_\odot\ {\rm pc}^{-2}$ and the four choices of $r_{\rm tn} = 2.0$ kpc, 2.5 kpc, 3 kpc, and 3.5 kpc. We display in Tables 1–7 the parameters characterizing the dark matter distribution that fit the rotation curve. We show in Figure 3 a selection of better-fitting models for the rotation curve (i.e., that pass through the shaded band) for each of these sets of models. The corresponding density profiles for these models are shown in Figure 4. The local and central dark matter density, the escape velocity from the R_0 and from the Galactic center, and the rms velocity at R_0 for each of these models are also presented in Tables 1–7.

The following points may be noted after a perusal of the figures and tables:

1. None of the dark matter models were found to be consistent with the rotation curve for a thin disk scale length of 2.0 kpc. For all choices of PSD parameters, the calculated rotation curves were less than 220 km s^{-1} at R_0. To be
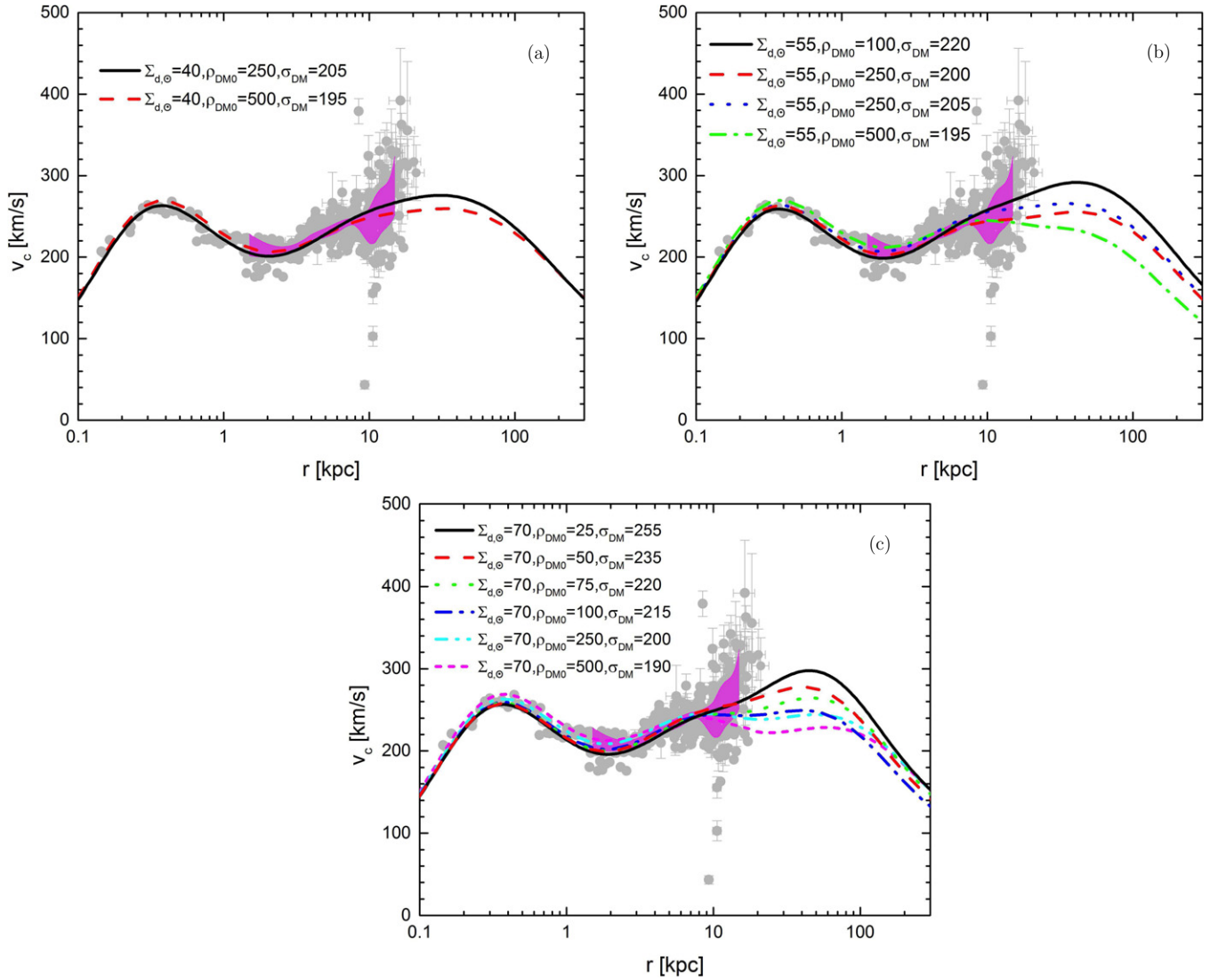
Figure 3. Rotation curves are shown for the dark matter models which pass through the band encompassing 2/3 of the observations in 1 kpc bins for $r_{tn} = 3.0$ kpc and (a) $\Sigma_{d,\odot} = 40\ M_\odot$ pc^{-2}, (b) $\Sigma_{d,\odot} = 55\ M_\odot$ pc^{-2}, and (c) $\Sigma_{d,\odot} = 70\ M_\odot$ pc^{-2}.

(A color version of this figure is available in the online journal.)

consistent with the rotation curve, a visible disk with $r_{tn} = 2.0$ kpc would have to have a local surface density that falls outside observational constraints. For $r_{tn} = 2.5$ kpc, only the lightest disk produced dark matter models consistent with the rotation curve.

2. All the models presented in Tables 1–7 provide good fits to the observed rotation curve within the solar circle ($r < R_0$).

3. The larger the assumed value of the surface density of the disk, the larger is the range of allowed parameters of the dark matter distributions.

4. The range in the parameters allowed by all the various models that best fit the rotation curve is:

   (a) 872.1 km s$^{-1} \lesssim v_{esc}(0) \lesssim 983.9$ km s^{-1}
   (b) 506.3 km s$^{-1} \lesssim v_{esc}(R_0) \lesssim 705.0$ km s^{-1}
   (c) 25 GeV cm$^{-3} \lesssim \rho_{DM,c} \lesssim 500$ GeV cm^{-3}
   (d) 0.395 GeV cm$^{-3} \lesssim \rho_{DM}(R_0) \lesssim 0.760$ GeV cm^{-3}
   (e) 392.2 km s$^{-1} \lesssim \langle v_{DM}^2(R_0)\rangle^{1/2} \lesssim 546.1$ km s^{-1}
   (f) $0.61 \times 10^{12}\ M_\odot \lesssim M_{Galaxy} \lesssim 2.00 \times 10^{12}\ M_\odot$.

5. Even though we plan to discuss elsewhere the implications of these results for direct and indirect detection of dark

matter, we may note here that the range in expected signals is large and the local dark matter density for every model is greater than the standard IAU value of 0.3 GeV cm^{-3}. However, an assumption of a lower value of Θ_0 would lead to a lower expectation for the dark matter density. The signals for direct detection are directly proportional to $\rho_{DM}(R_0)$ and increase at least linearly with $\langle v_{DM}^2(R_0)\rangle^{1/2}$, so that the allowed rate may vary at least by ~8, even for detectors with very low threshold. The indirect experiments focus usually on detecting annihilation or decay of dark matter from the central regions of the Galaxy. These rates, proportional to $\rho_{DM}^2(0)$ and $\rho_{DM}(0)$, span a range of 400 and 20, respectively.

6. To investigate the correlations among the various parameters and derived quantities of the dark matter models given in Tables 1–7, the values of σ_{DM}, $\langle v_{DM}^2(R_0)\rangle^{1/2}$, $\rho_{DM}(R_0)$, $v_{esc}(0)$, and $v_{esc}(R_0)$ are plotted as a function of the central dark matter density, $\rho_{DM,c}$, in Figures 5(a)–(e). Also shown is the dark matter density in the solar neighborhood as a function of $\langle v_{DM}^2(R_0)\rangle^{1/2}$ in Figure 5(f). The following observations may be made:
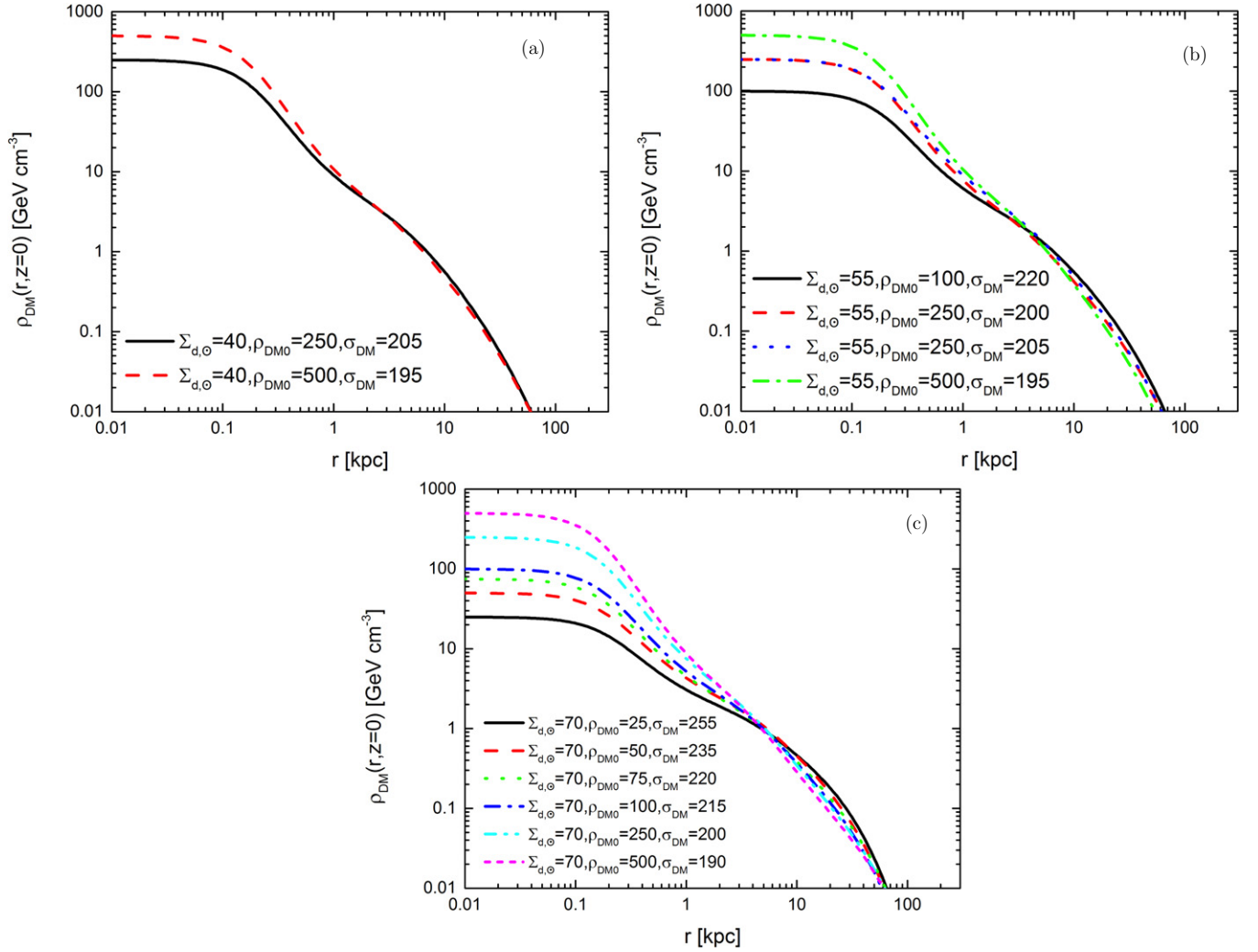
Figure 4. Density profiles for dark matter models that best fit the rotation curve are shown for r_{tn} and (a) $\Sigma_{d,\odot} = 40 \ M_\odot \ \mathrm{pc}^{-2}$, (b) $\Sigma_{d,\odot} = 55 \ M_\odot \ \mathrm{pc}^{-2}$, and (c) $\Sigma_{d,\odot} = 70 \ M_\odot \ \mathrm{pc}^{-2}$.
(A color version of this figure is available in the online journal.)

Table 3
Dark Matter Model Parameters and Derived Quantities for the $r_{tn} = 3.0$ and $\Sigma_{d,\odot} = 55 \ M_\odot \ \mathrm{pc}^{-2}$ Disk

$\rho_{\mathrm{DM},c}$ (GeV cm^{-3})	25	50	75	100	250	500
σ_{DM} (km s^{-1})	⋯	⋯	⋯	220	200	195
	⋯	⋯	⋯	⋯	205	⋯
$\Psi_0/\sigma_{\mathrm{DM}}^2$	⋯	⋯	⋯	10	11	11
	⋯	⋯	⋯	⋯	11	⋯
$v_{\mathrm{esc}}(0)$ (km s^{-1})	⋯	⋯	⋯	984	938	915
	⋯	⋯	⋯	⋯	962	⋯
$v_c(R_0)$ (km s^{-1})	⋯	⋯	⋯	251	241	245
	⋯	⋯	⋯	⋯	252	⋯
$\langle v_{\mathrm{DM}}^2(R_0)\rangle^{1/2}$ (km s^{-1})	⋯	⋯	⋯	546	489	443
	⋯	⋯	⋯	⋯	508	⋯
$\rho_{\mathrm{DM}}(R_0)$ (GeV cm^{-3})	⋯	⋯	⋯	0.719	0.563	0.535
	⋯	⋯	⋯	⋯	0.654	⋯
$v_{\mathrm{esc}}(R_0)$ (km s^{-1})	⋯	⋯	⋯	705	631	571
	⋯	⋯	⋯	⋯	656	⋯
M_{galaxy} ($10^{12} \ M_\odot$)	⋯	⋯	⋯	2.00	1.60	1.06
	⋯	⋯	⋯	⋯	1.68	⋯
L	⋯	⋯	⋯	1	0.732	0
	⋯	⋯	⋯	⋯	0.834	⋯

Note. See the caption of Figure 1 for details.

Table 4
Dark Matter Model Parameters and Derived Quantities for the $r_{tn} = 3.0$ and $\Sigma_{d,\odot} = 70 \ M_\odot \ \mathrm{pc}^{-2}$ Disk

$\rho_{\mathrm{DM},c}$ (GeV cm^{-3})	25	50	75	100	250	500
σ_{DM} (km s^{-1})	255	235	220	215	200	190
$\Psi_0/\sigma_{\mathrm{DM}}^2$	7	8	9	9	11	12
$v_{\mathrm{esc}}(0)$ (km s^{-1})	954	940	933	912	938	931
$v_c(R_0)$ (km s^{-1})	244	248	243	243	246	241
$\langle v_{\mathrm{DM}}^2(R_0)\rangle^{1/2}$ (km s^{-1})	520	498	491	463	481	463
$\rho_{\mathrm{DM}}(R_0)$ (GeV cm^{-3})	0.573	0.582	0.505	0.489	0.470	0.395
$v_{\mathrm{esc}}(R_0)$ (km s^{-1})	671	643	634	598	621	597
M_{galaxy} ($10^{12} \ M_\odot$)	1.69	1.46	1.58	1.27	1.67	1.69
L	0.524	0.250	0.597	0.056	0.784	0.764

Note. See the caption of Figure 1 for details.

(a) The correlation between the central density $\rho_{\mathrm{DM},c}$ and the value of the σ_{DM} parameter is shown in Figure 5(a), and the value of σ_{DM} is shown to decrease with increasing $\rho_{\mathrm{DM},c}$. The decrease becomes progressively more gentle, and σ_{DM} reaches a values of $\sim$195 km s^{-1} at $\rho_{\mathrm{DM},c} = 500$ GeV cm^{-3}.
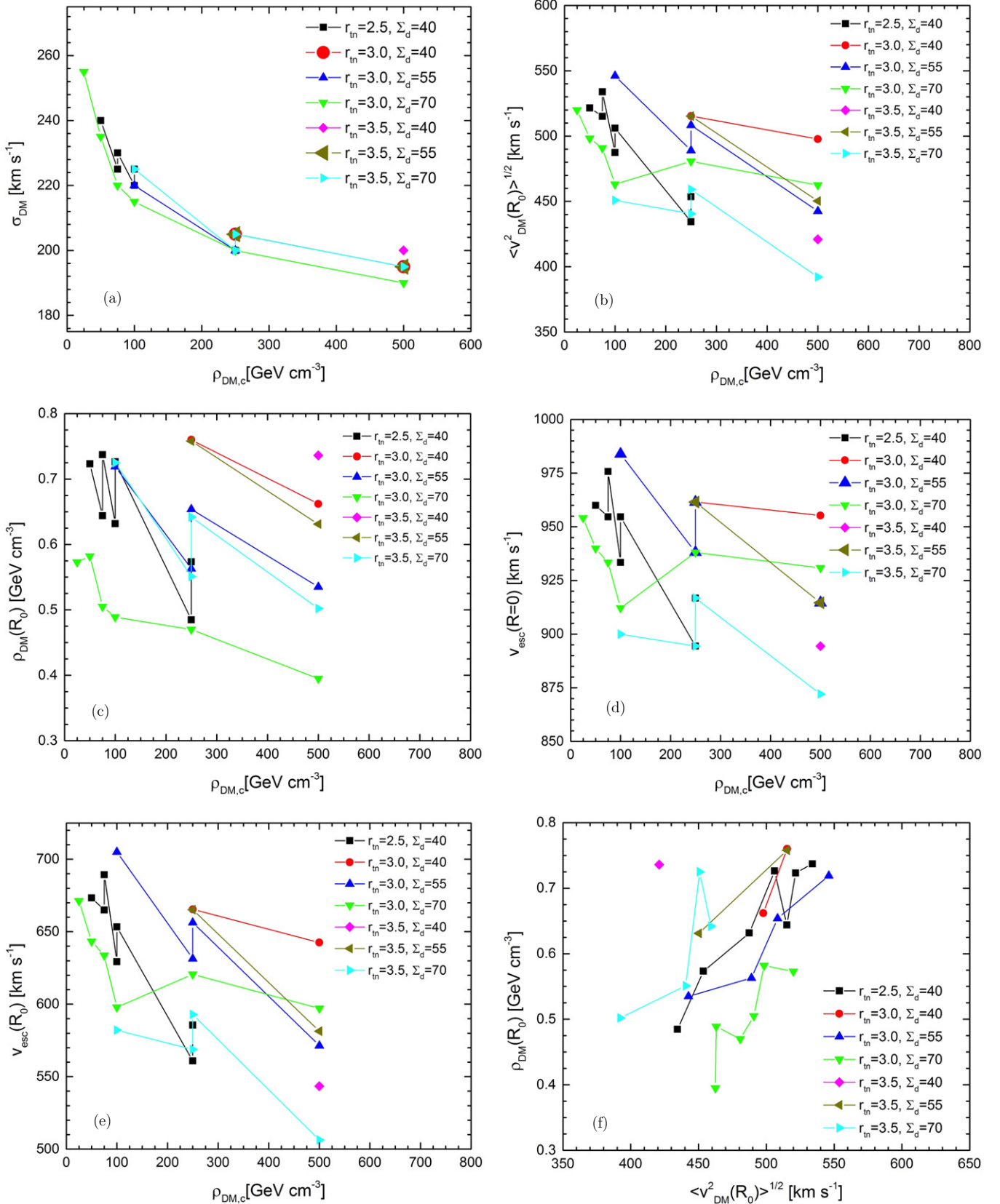
Figure 5. Correlation between the various model parameters of dark matter that fit the rotation curve of the Galaxy.

(A color version of this figure is available in the online journal.)

Table 5
Dark Matter Model Parameters and Derived Quantities for the $r_{tn} = 3.5$ and $\Sigma_{d,\odot} = 40\ M_\odot\ pc^{-2}$ Disk

$\rho_{DM,c}$ (GeV cm^{-3})	25	50	75	100	250	500
σ_{DM} (km s^{-1})	...	...	...	...	...	200
Ψ_0/σ^2_{DM}	...	...	...	...	...	10
$v_{esc}(0)$ (km s^{-1})	...	...	...	...	...	894
$v_c(R_0)$ (km s^{-1})	...	...	...	...	...	251
$\langle v^2_{DM}(R_0)\rangle^{1/2}$ (km s^{-1})	...	...	...	...	...	421
$\rho_{DM}(R_0)$ (GeV cm^{-3})	...	...	...	...	...	0.736
$v_{esc}(R_0)$ (km s^{-1})	...	...	...	...	...	544
M_{galaxy} ($10^{12}\ M_\odot$)	...	...	...	...	...	0.67
L	...	...	...	...	...	0

Note. See the caption of Table 1 for details.

Table 6
Dark Matter Model Parameters and Derived Quantities for the $r_{tn} = 3.5$ and $\Sigma_{d,\odot} = 55\ M_\odot\ pc^{-2}$ Disk

$\rho_{DM,c}$ (GeV cm^{-3})	25	50	75	100	250	500
σ_{DM} (km s^{-1})	...	...	...	...	205	195
Ψ_0/σ^2_{DM}	...	...	...	...	11	11
$v_{esc}(0)$ (km s^{-1})	...	...	...	...	962	915
$v_c(R_0)$ (km s^{-1})	...	...	...	...	254	246
$\langle v^2_{DM}(R_0)\rangle^{1/2}$ (km s^{-1})	...	...	...	...	515	450
$\rho_{DM}(R_0)$ (GeV cm^{-3})	...	...	...	...	0.758	0.631
$v_{esc}(R_0)$ (km s^{-1})	...	...	...	...	665	581
M_{galaxy} ($10^{12}\ M_\odot$)	...	...	...	...	1.61	1.02
L	...	...	...	...	0.781	0

Note. See the caption of Table 1 for details.

Table 7
Dark Matter Model Parameters and Derived Quantities for the $r_{tn} = 3.5$ and $\Sigma_{d,\odot} = 70\ M_\odot\ pc^{-2}$ Disk

$\rho_{DM,c}$ (GeV cm^{-3})	25	50	75	100	250	500
σ_{DM} (km s^{-1})	...	...	...	225	200	195
	...	...	...	...	205	...
Ψ_0/σ^2_{DM}	...	...	...	8	10	10
	...	...	...	...	10	...
$v_{esc}(0)$ (km s^{-1})	...	...	...	900	894	872
	...	...	...	...	917	...
$v_c(R_0)$ (km s^{-1})	...	...	...	256	243	245
	...	...	...	...	254	...
$\langle v^2_{DM}(R_0)\rangle^{1/2}$ (km s^{-1})	...	...	...	451	441	392
	...	...	...	...	459	...
$\rho_{DM}(R_0)$ (GeV cm^{-3})	...	...	...	0.725	0.551	0.502
	...	...	...	...	0.642	...
$v_{esc}(R_0)$ (km s^{-1})	...	...	...	582	569	506
	...	...	...	...	593	...
M_{galaxy} ($10^{12}\ M_\odot$)	...	...	...	0.84	0.98	1.04
	...	...	...	...	0.61	...
L	...	...	...	0	0	0
	...	...	...	...	0	...

Note. See the caption of Table 1 for details.

(b) The rms velocities of the dark matter particles near the solar system, $\langle v^2_{DM}(R_0)\rangle^{1/2}$, decrease with respect to $\rho_{DM,c}$ as shown in Figure 5(b).

(c) Similarly, the dark matter density at R_0 decreases gently with respect to $\rho_{DM,c}$ as shown in Figure 5(c).

(d) The escape velocity from the center of the Galaxy and from the location of the solar system gently decreases beyond $\rho_{DM,c} \sim 200$ GeV cm^{-3} for a given set of disk parameters (see Figures 5(d) and (e)).

(e) The value of $\rho_{DM}(R_0)$ increases statistically with increasing $\langle v^2_{DM}(R_0)\rangle^{1/2}$ as shown in Figure 5(f), thereby increasing the range of expectation of event rates in direct detection experiments.

7. After solving Poisson's equation, the potential at every point in the Galaxy is known. It is therefore possible to calculate the force profile in any direction. In Figure 6, the vertical force profile at the solar location is shown for a selection of the dark matter models that provide a good fit to the observations of the rotation curve. With more extensive astronomical observations, the motions of stars above the Galactic plane at R_0 could be used to further constrain the dark matter parameters and the surface density of the disk in the neighborhood of the Sun.

5.2. Comparison with the Distributions of BHB and BS Stars

The BHB and BS stars, with their distribution extending up to ~90 kpc, serve as tracers of the gravitational potential of the Galaxy, even though they contribute negligibly to the potential. Since only their radial velocities are well determined, we will first write down their radial distribution function under the

assumption that their PSD function follows the King distribution such as that given in Equation (13). This is achieved by writing $\Psi(r) = (1/2)v^2_{esc}(r)$ and integrating the PSD function over the transverse velocities:

$$F_B(r, v_r) = \frac{\rho_B}{\left(2\pi\sigma_B^2\right)^{3/2}}$$
$$\times \int_0^{v^2_{esc}(r)-v_r^2} \left[\exp\left(\frac{v^2_{esc}(r) - v_r^2 - v_\perp^2}{2\sigma_B^2}\right) - 1\right]\pi dv_\perp^2 \tag{20}$$

$$= \frac{\pi\rho_B}{\left(2\pi\sigma_B^2\right)^{3/2}}\left\{2\sigma_B^2\left[\exp\left(\frac{v^2_{esc}(r) - v_r^2}{2\sigma_B^2}\right) - 1\right]\right.$$
$$\left. - \left(v^2_{esc}(r) - v_r^2\right)\right\}dv_r. \tag{21}$$

The expression given in Equation (21) is suitable for comparison with the observed distributions. However, the samples of BHB and BS stars (Xue et al. 2008; Brown et al. 2010) appear to be incomplete, at least with regard to radial sampling. In order to assess this, we integrate $F_B(r, v_r)$ over the radial velocities to get the radial distribution of number density, which is given by

$$n_B(r) = \int_0^{v_{esc}(r)} F_B(r, v_r)dv_r \tag{22}$$

$$= \frac{\rho_B}{\left(2\pi\sigma_B^2\right)^{3/2}}\left[\frac{\left(2\pi\sigma_B^2\right)^{3/2}}{2}e^{v^2_{esc}(r)/2\sigma_B^2}\mathrm{erf}\left(\frac{v_{esc}(r)}{\sqrt{2\sigma_B^2}}\right)\right.$$
$$\left. - \frac{2\pi}{3}v^3_{esc}(r) - 2\pi\sigma_B^2 v_{esc}(r)\right]. \tag{23}$$

The number of stars in unit radial interval at r is then given by

$$N(r) = 4\pi r^2 n_B(r). \tag{24}$$

The distributions of BHB and BS stars with $\sigma_B = 106$ km s^{-1} for the Xue et al. (2008) BHB stars and $\sigma_B = 115$ km s^{-1}
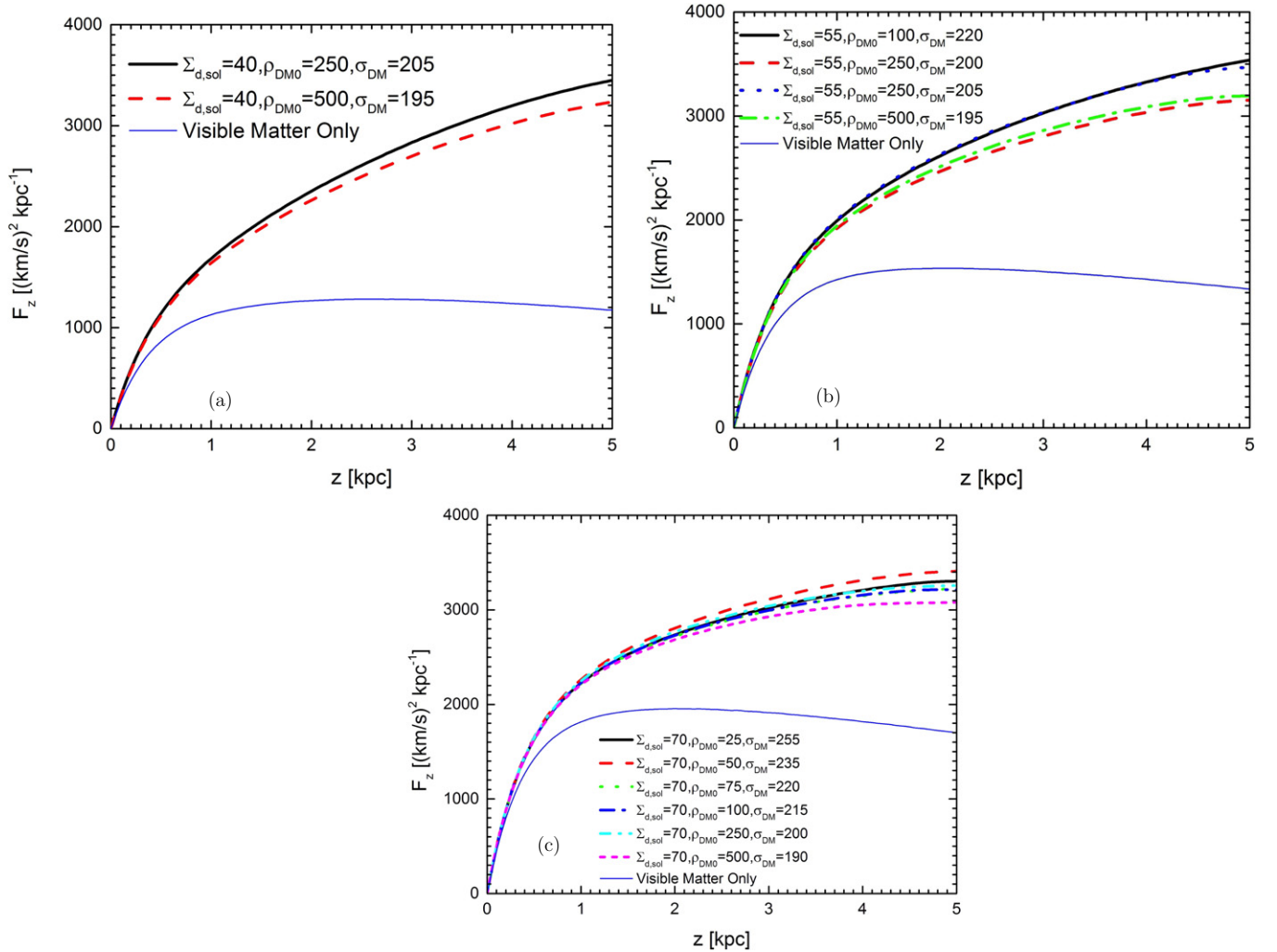
Figure 6. Vertical force profiles at the galactocentric distance of the Sun for dark matter models that best fit the rotation curve are shown for $r_{tn} = 3.0$ kpc and (a) $\Sigma_{d,\odot} = 40\ M_\odot\ \mathrm{pc}^{-2}$, (b) $\Sigma_{d,\odot} = 55\ M_\odot\ \mathrm{pc}^{-2}$, and (c) $\Sigma_{d,\odot} = 70\ M_\odot\ \mathrm{pc}^{-2}$.
(A color version of this figure is available in the online journal.)

for the Brown et al. (2010) BHB and BS stars calculated for the best-fitting model with $\Sigma_{d,\odot} = 55\ M_\odot\ \mathrm{pc}^{-2}$ are shown in Figure 7. A single choice for the parameter ρ_B should, in principle, fit the total number of stars observed in each radial bin when we include all the stars at that location irrespective of their velocities. Unfortunately, this does not happen, and the observed number of stars, especially at galactocentric distances below ∼20–30 kpc, falls short of the theoretical expectation. The most likely explanation for this is that the samples of BS and BHB stars are incomplete in these regions. In fact, the radial distributions presented by Xue et al. (2008) and Brown et al. (2010) also differ significantly from each other. We therefore integrate $4\pi r^2 F_B(r, v_r)$ over radial location and radial velocity, $\Delta r(r_i)$ and $\Delta v_r(r_i, v_j)$, respectively, and compare it with similarly binned observational data after normalizing the model estimates to the total number of stars observed in each individual bin separately. A selection of the fits is shown in Figures 8 and 9 for the disk model with $r_{tn} = 3.0$ kpc and $\Sigma_{d,\odot} = 55\ M_\odot$.

For finding out how well the different models fit the observations, we define f_{ij} as the theoretical expectation for the number of stars in the radial bin r_i and the velocity bin v_{rj}. If n_{ij} is the actual number of stars observed in this bin, then, using Poisson statistics, we may define the likelihood function for each model
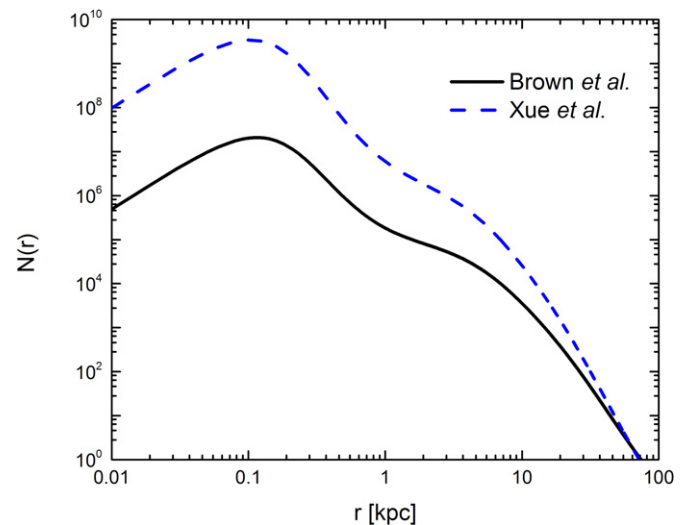

Figure 7. Theoretical radial distributions of BHB and BS stars expected from the velocity distribution measured by Brown et al. and Xue et al. The distribution is shown for the $\Sigma_{d,\odot} = 55\ M_\odot\ \mathrm{pc}^{-2}$, $r_{tn} = 3.0$ kpc disk with $\rho_{DM,c} = 100$ GeV cm^{-3}, $\sigma_{DM} = 220$ km s^{-1}, and $\sigma_{BHB} = \sigma_{BS} = 115$ km s^{-1} for Brown et al. and $\sigma_{BHB} = 106$ km s^{-1} for Xue et al.
(A color version of this figure is available in the online journal.)
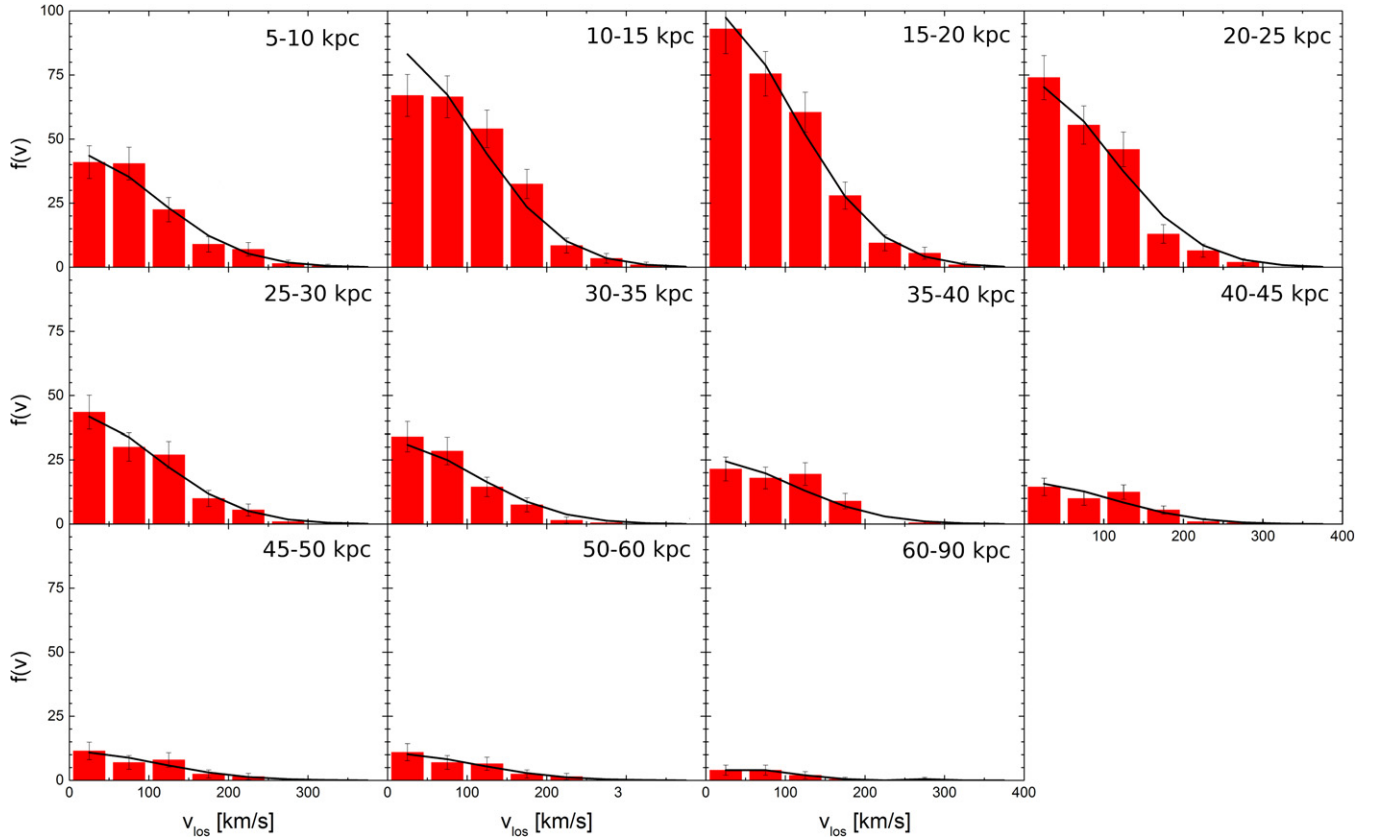
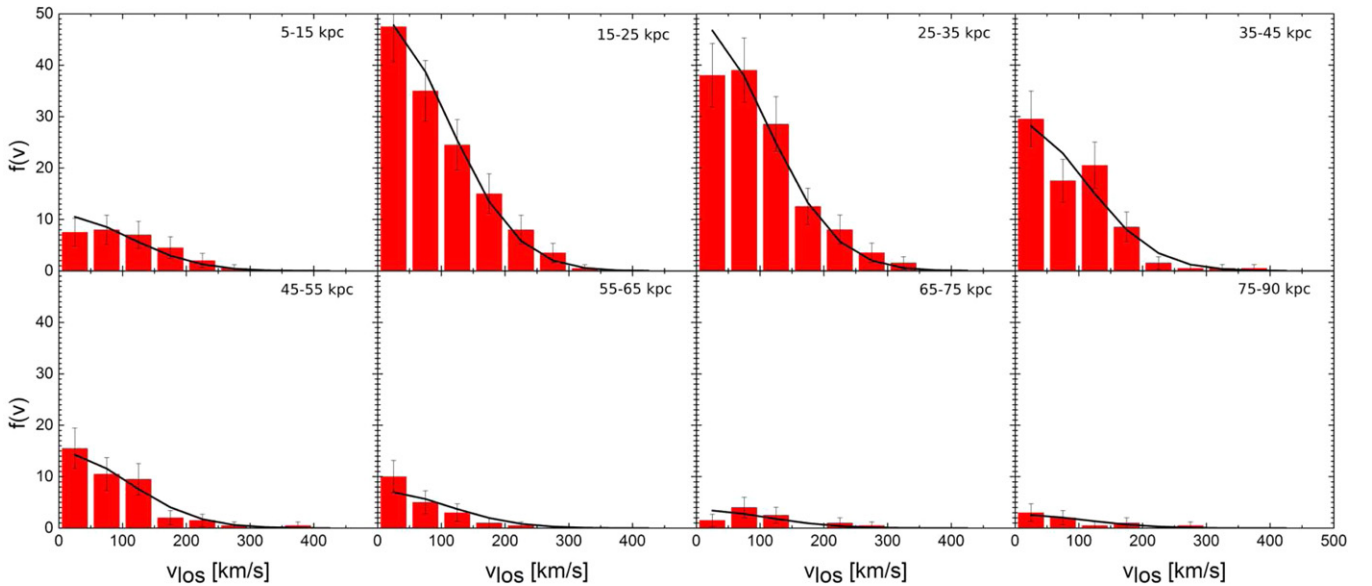**Figure 8.** Line-of-sight velocity distribution of BHB stars from Xue et al. (2008) is presented in radial velocity and radial bins in the red histogram with error bars. The distribution computed for the best-fit dark matter model for the $\Sigma_{d,\odot} = 55\ M_\odot\ \mathrm{pc}^{-2}$, $r_{\mathrm{tn}} = 3.0$ kpc disk is shown as points, connected for clarity. In this model, $\rho_{\mathrm{DM},c} = 100\ \mathrm{GeV\ cm}^{-3}$, $\sigma_{\mathrm{DM}} = 220\ \mathrm{km\ s}^{-1}$, $\Phi_0/\sigma_{\mathrm{DM}}^2 = 10$, and $\sigma_{\mathrm{BHB}} = 106\ \mathrm{km\ s}^{-1}$.

(A color version of this figure is available in the online journal.)

Figure 9. Line-of-sight velocity distribution of BHB and BS stars from Brown et al. (2010) is presented in radial velocity and radial bins in the red histogram with error bars. The distribution computed for the best-fit dark matter model for the $\Sigma_{d,\odot} = 55\ M_\odot\ \mathrm{pc}^{-2}$, $r_{\mathrm{tn}} = 3.0$ kpc disk is shown as points, connected for clarity. In this model, $\rho_{\mathrm{DM},c} = 200\ \mathrm{GeV\ cm}^{-3}$, $\sigma_{\mathrm{DM}} = 230\ \mathrm{km\ s}^{-1}$, $\Phi_0/\sigma_{\mathrm{DM}}^2 = 10$, and $\sigma_{\mathrm{BHB,BS}} = 115\ \mathrm{km\ s}^{-1}$.

(A color version of this figure is available in the online journal.)

to be

$$L = \prod_{ij} \frac{e^{-f_{ij}} f_{ij}^{n_{ij}}}{n_{ij}!}. \qquad (25)$$

After the likelihoods for all the models were calculated, they were normalized to the model with the greatest likelihood, namely, with $\rho_{\mathrm{DM},c} = 100\ \mathrm{GeV\ cm}^{-3}$, $\sigma_{\mathrm{DM}} = 220\ \mathrm{km\ s}^{-1}$, $\Sigma_{d,\odot} = 55\ M_\odot\ \mathrm{pc}^{-2}$, and $r_{\mathrm{tn}} = 3.0$ kpc. The likelihood for each

dark matter model that fits the rotation curve is shown in the final rows of Tables 1–7.

Most of the models with high probability, according to the BHB and BS analysis, occur for $\rho_{DM,c} \gtrsim 100$ GeV cm^{-3}. Also, except for two specific cases, one in each of the $r_{tn} = 2.5$ and 3.5 kpc scenarios, the models with $L > 0.7$ are found for the choice $r_{tn} = 3.0$ kpc. All models with $L > 0.8$ are found for $r_{tn} = 3.0$ kpc and $\Sigma_{d,\odot} = 55\ M_\odot$ pc^{-2}. Most models for the $r_{tn} = 3.5$ kpc disk, though they fit the rotation curve, do not predict enough stars at large velocities to agree with the BHB and BS data (note the sharply falling rotation curves at large distances in these models) and have a likelihood $L = 0$.

If we consider only the models with $L > 0.7$, we find the following range in the parameters for the dark matter particles in the Galaxy:

$$930.8\,\text{km s}^{-1} \lesssim v_{esc}(0) \lesssim 983.9\,\text{km s}^{-1}$$

$$597.1\,\text{km s}^{-1} \lesssim v_{esc}(R_0) \lesssim 705.0\,\text{km s}^{-1}$$

$$75\,\text{GeV cm}^{-3} \lesssim \rho_{DM,c} \lesssim 500\,\text{GeV cm}^{-3}$$

$$0.395\,\text{GeV cm}^{-3} \lesssim \rho_{DM}(R_0) \lesssim 0.758\,\text{GeV cm}^{-3}$$

$$462.5\,\text{km s}^{-1} \lesssim \langle v_{DM}^2(R_0)\rangle^{1/2} \lesssim 546.1\,\text{km s}^{-1}$$

$$1.60 \times 10^{12}\,M_\odot \lesssim M_{Galaxy} \lesssim 2.00 \times 10^{12}\,M_\odot.$$

6. DISCUSSION

While the observations of the rotation curve remain the best probes of the Galactic potential out to $\sim$20 kpc, the high dispersion in the observed rotation speeds, especially at large distances, does not allow a precise determination of the parameters characterizing the PSD of Galactic dark matter. Among the models where the rotation curve is confined to lie within a narrow band encompassing 2/3 of the observed data, a wide range in the parameters is allowed, as shown in Tables 1–7 and Figures 3–6. It may be possible to further constrain the dark matter PSD by comparing the vertical force exerted by the Galactic potential at R_0 displayed for several models in Figure 6 with the stellar observations perpendicular to the plane in the solar neighborhood as an extension of the analysis by Kuijken & Gilmore (1989).

The model providing the best fit for disks with surface densities within observational constraints to both the rotation curve and the BHB/BS distributions occurs for the following dark matter PSD parameters: $\rho_{DM,c} = 100$ GeV cm^{-3}, $\Psi_0/\sigma_{DM}^2 = 10$, and $\sigma_{DM} = 220$ km s^{-1}. The corresponding properties of the dark matter relevant to its direct detection are $\langle v^2(R_0)_{DM}\rangle^{1/2} \approx 546$ km s^{-1} and $\rho_{DM}(R_0) \approx 0.72$ GeV cm^{-3}. This local dark matter density is notably higher than the currently adopted Standard Halo Model. The effect this increase has on the expected rates of direct and indirect detection predictions will be discussed in a companion paper.

Better observations of the distance of the Sun from the Galactic center and the value of the rotation speed at the solar circle, as well as observations of the rotation curve beyond R_0,

especially at distances beyond 20 kpc, would allow for better constraints on the PSD of dark matter. The currently observed distributions of BHB and BS stars have large uncertainties as to their absolute spatial densities and do not place tight bounds on the dark matter PSD on their own. This was shown by the wide range of dark matter models that adequately reproduced the velocity distributions at various distances compiled by Xue et al. and Brown et al. The wide range of allowed parameters shows that more precise astronomical observations, especially pertaining to the surface mass density of the disk and its radial scale length, are needed to narrow down the parameters of the PSD of dark matter and to be able to correctly interpret the results of direct and indirect dark matter detection experiments. As far as the present status of the observations is concerned, assuming that the surface density of the Galactic disk is $\sim$55 $M_\odot$ pc^{-2}, a value in the middle of the observational constraints, and a thin disk scale length of 3.0 kpc, the best choices for the parameters of Galactic dark matter ($L > 0.7$) are the following: $\rho_{DM,c} \approx 100$–250 GeV cm^{-3}, $\rho_{DM}(R_0) \approx 0.56$–0.72 GeV cm^{-3}, and $\langle v_{DM}^2(R_0)\rangle^{1/2} \approx 490$–550 km s^{-1}, which yield a total mass of the Galaxy including the dark matter halo of $M_{Galaxy} \approx (1.68$–$2.00) \times 10^{12}\ M_\odot$.

REFERENCES

Ahmed, Z., Akerib, D. S., Arrenberg, S., et al. 2011, PhRvL, 106, 131302
Aprile, E., Alfonsi, M., Arneodo, F., et al. 2012, PhRvL, 109, 181301
Archambault, S., Behnke, E., Bhattacharjee, P., et al. 2012, PhLB, 711, 153
Avedisova, V. S. 2005, ARep, 49, 435
Bahcall, J. N., & Soneira, R. M. 1980, ApJS, 44, 73
Behnke, E., Behnke, J., Brice, S. J., et al. 2011, PhRvL, 106, 021303
Bensby, T., Alves-Brito, A., Oey, M. S., Yong, D., & Meléndez, J. 2011, ApJ, 735, L46
Bhattacharjee, P., Chaudhury, S., Kundu, S., & Majumdar, S. 2013, PhRvD, 87, 083525
Binney, J., & Tremaine, S. 2008, Galactic Dynamics (2nd ed.; Princeton, NJ: Princeton Univ. Press)
Blitz, L., Fich, M., & Stark, A. A. 1982, ApJS, 49, 183
Blum, R. D., Carr, J. S., Sellgren, K., & Terndrup, D. M. 1995, ApJ, 449, 623
Bovy, J., Prieto, C. A., Beers, T. C., et al. 2012a, ApJ, 759, 131
Bovy, J., Rix, H., Chao, L., et al. 2012b, ApJ, 753, 148
Bovy, J., & Tremaine, S. 2012, AJ, 756, 89
Brown, W. R., Geller, M. J., Kenyon, S. J., & Diaferio, A. 2010, ApJ, 139, 59
Brunthaler, A., Reid, M. J., Menten, K. M., et al. 2011, AN, 332, 461
Burton, W. B., & Gordon, M. A. 1978, A&A, 63, 7
Burton, W. B., & Liszt, H. S. 1993, A&A, 274, 765
Buser, R., Rong, J., & Karaali, S. 1999, A&A, 348, 98
Cabrera-Lavers, A., Garzón, F., & Hammersley, P. L. 2005, A&A, 433, 173
Caldwell, J. A. R., & Ostriker, J. P. 1981, AJ, 251, 61
Carollo, D., Beers, T. C., Chiba, M., et al. 2010, ApJ, 712, 692
Catena, R., & Ullio, P. 2010, JCAP, 08, 004
Catena, R., & Ullio, P. 2012, JCAP, 05, 005
Chaudhury, S., Bhattacharjee, P., & Cowsik, R. 2010, JCAP, 09, 020
Cheng, J. Y., Rockosi, C. M., Morrison, H. L., et al. 2012, ApJ, 752, 51
Clemens, D. P. 1985, ApJ, 295, 422
Cowsik, R., & McClelland, J. 1972, PhRvL, 29, 669
Cowsik, R., & McClelland, J. 1973, ApJ, 180, 7
Cowsik, R., Ratnam, C., & Bhattacharjee, P. 1996, PhRvL, 76, 3886
Cowsik, R., Ratnam, C., Bhattacharjee, P., & Majumdar, S. 2007, NewA, 12, 507
Dehnen, W., & Binney, J. 1998, MNRAS, 294, 429
Dejonghe, H. 1987, MNRAS, 224, 12
Demers, S., & Battinelli, P. 2007, A&A, 473, 143
Felizardo, M., Girard, T. A., Morlat, T., et al. 2012, PhRvL, 108, 201302
Fich, M., Blitz, L., & Stark, A. A. 1989, ApJ, 342, 272
Flynn, C., & Fuchs, B. 1994, MNRAS, 270, 471
Flynn, C., Holmberg, J., Portinari, L., et al. 2006, MNRAS, 372, 1149
Freeman, K. C. 1970, ApJ, 160, 811
Ghez, A. M., Salim, S., Weinberg, N. N., et al. 2008, ApJ, 689, 1044
Gillessen, S., Eisenhauer, F., Trippe, S., et al. 2009, ApJ, 692, 1075
Gould, A., Bahcall, J. N., & Flynn, C. 1996, ApJ, 465, 759
Helmi, A. 2008, A&AR, 15, 145

Holmberg, J., & Flynn, C. 2004, MNRAS, 352, 440
Honma, M., Bushimata, T., Choi, Y. K., et al. 2007, PASJ, 59, 889
Honma, M., & Sofue, Y. 1997, PASJ, 49, 453
Jurić, M., Ivezić, Ž., Brooks, A., et al. 2008, ApJ, 673, 864
Kolb, E., & Turner, M. 1990, The Early Universe (Redwood City, CA: Addison-Wesley)
Koposov, S. E., Rix, H., & Hogg, D. 2010, ApJ, 712, 260
Korchagin, V. I., Girard, T. M., Borkova, T. V., Dinescu, D. I., & van Altena, W. F. 2003, ApJ, 126, 2896
Kuhlen, M., Weiner, N., Diemand, J., et al. 2010, JCAP, 02, 030
Kuijken, K., & Gilmore, G. 1989, MNRAS, 239, 605
Kuijken, K., & Gilmore, G. 1991, ApJL, 367, L9
Larsen, J. A., & Humphreys, R. M. 2003, AJ, 125, 1958
Lee, B. W., & Weinberg, S. 1977, PhRvL, 39, 165
Libeskind, N. I., Knebe, A., Hoffman, Y., et al. 2011, MNRAS, 411, 1525
McClure-Griffiths, N. M., & Dickey, J. M. 2007, ApJ, 671, 427
McMillan, P. J. 2011, MNRAS, 414, 2446
McMillan, P. J., & Binney, J. J. 2010, MNRAS, 402, 934
Minniti, D., White, S. D. M., Olszewski, E., & Hill, J. 1992, ApJ, 393, L47
Mo, H., van den Bosch, F., & White, S. 2010, Galaxy Formation and Evolution (Cambridge: Cambridge Univ. Press)
Navarro, J. F., Frenk, C. S., & White, S. D. M. 1997, ApJ, 490, 493
Nesti, F., & Salucci, P. 2013, JCAP, 07, 016
Ng, Y. K., Bertelli, G., Chiosi, C., & Bressan, A. 1997, A&A, 324, 65
Oh, C. S., Kobayashi, H., Honma, M., et al. 2010, PASJ, 62, 101
Ojha, D. K. 2001, MNRAS, 322, 426

Oort, J. 1932, BAN, 6, 249
Pont, F., Queloz, D., Bratschi, P., & Mayor, M. 1997, A&A, 318, 416
Prendergast, K. H., & Tomer, E. 1970, AJ, 75, 674
Reid, M. J. 2009, IJMPD, 18, 889
Reid, M. J., & Brunthaler, A. 2004, ApJ, 616, 872
Reid, M. J., Menten, K. M., Zheng, X. W., et al. 2008, ApJ, 700, 137
Reid, N., & Majewski, S. R. 1993, ApJ, 409, 635
Rich, R. M., Reitzel, D. B., Howard, C. D., & Zhao, H. 2007, ApJ, 658, L29
Robin, A. C., Haywood, M., Creze, M., Ojha, D. K., & Bienayme, O. 1996, A&A, 305, 125
Rohlfs, K., & Kreitschmann, J. 1988, A&A, 201, 51
Salucci, P., Nesti, F., Gentile, G., & Frigerio Martins, C. 2010, A&A, 523, 83
Schmidt, M. 1956, BAN, 13, 15
Schneider, S. E., & Terzian, Y. 1983, ApJL, 274, L61
Schönrich, R., Binney, J., & Dehnen, W. 2010, MNRAS, 403, 1829
Siebert, A., Bienaymé, O., & Soubiran, C. 2003, A&A, 399, 531
Siegel, M. H., Majewski, S. R., Reid, I. N., & Thompson, I. B. 2002, ApJ, 578, 151
Sofue, Y., Honma, M., & Omodaka, T. 2009, PASJ, 61, 227
Spagna, A., Lattanzi, M. G., Lasker, B. M., et al. 1996, A&A, 311, 758
Stepanishchev, A. S., & Bobylev, V. V. 2011, AstL, 37, 254
Turbide, L., & Moffat, A. F. J. 1993, AJ, 105, 1831
Weber, W., & de Boer, W. 2010, A&A, 509, A25
Wilson, C. P. 1975, ApJ, 80, 175
Xue, X. X., Rix, H. W., Re Fiorentin, R., et al. 2008, ApJ, 684, 1143